INTERNATIONAL JOURNAL FOR NUMERICAL METHODS IN FLUIDS, VOL. 8, 387–404 (1988)

EXAMINATION OF PRESSURE OSCILLATIONS ARISING IN THE COMPUTATION OF CASCADE FLOW USING A BOUNDARY-FITTED CO-ORDINATE SYSTEM

B. L. LAPWORTH

Turbomachinery Research Group, School of Mechanical Engineering, Cranfield Institute of Technology, Cranfield, Bedford, MK43 0AL U.K.

SUMMARY

The incompressible flow through a two-dimensional cascade is computed using the SIMPLE algorithm in a boundary-fitted co-ordinate system. With the standard staggered grid arrangement the numerical solution was found to allow localized pressure oscillations to persist adjacent to the periodic boundaries. These oscillations were found to be a consequence of the extended momentum control volumes which are required in this region of the cascade. Such control volumes may be removed by the use of appropriately non-staggered velocity storage locations, which are also desirable in the boundary-fitted system since the Cartesian velocity components are no longer related to the grid line orientations. However, this storage permits the propagation of global pressure oscillations, which were previously suppressed by the staggered grid arrangement. This paper attempts to define a solution procedure which uses non-staggered velocity locations and is able to eliminate the consequent global pressure oscillations. To achieve this aim, two forms of pressure correction scheme were considered. The first implemented the scheme proposed by Vanka *et al.* but was found to be inadequate in the open part of the cascade, whereas the second employed a modification of the scheme proposed by Rhie and Chow and was found to be successful in all regions of the flow. The results computed using this scheme were compared with the available experiment results.

KEY WORDS Boundary-fitted co-ordinates SIMPLE algorithm Non-staggered grid Cascade flow

INTRODUCTION

The bladings for turbomachines are amongst the most complex geometries that a flow may encounter. Consequently, there are many benefits in the accurate computation of the flow phenomena occurring within such geometries. Much of the early numerical modelling of turbomachinery flows was based on the stream surface procedure proposed by Wu.[1] By using the notion of intersecting stream surfaces, this procedure was able to deliver numerical results within the scope of the existing computational resources. This procedure is still widely used at present; but, with the many recent advances in computing power, it is no longer an unreasonable task to model the flow by solving the primitive Navier–Stokes equations. Indeed it is argued[2] that the introduction of the stream surfaces is a limiting influence on the accuracy of the numerical results and that a Navier–Stokes procedure is required for greater accuracy. Amongst the techniques to adopt this approach are the procedures proposed by Denton[3] and Moore and Moore.[4]

The present two-dimensional study is performed with the aim of defining a numerical solution procedure which is suitable for computing internal turbomachinery flows which are highly three-

0271–2091/88/040387–18$09·00

Received 4 February 1987
Revised 28 April 1987

dimensional in nature. With the anticipated advantages of a Navier–Stokes procedure in mind, the present computer code was developed from the CHAMPION code of Pun and Spalding.[5] This code solves finite volume approximations to the primitive variable flow equations using the SIMPLE algorithm of Patankar and Spalding.[6]

An important consideration in many solution algorithms is the choice of grid on which the flow equations are discretized. For the flow over a curved surface, such as a turbomachinery blade, the rigid axes of a Cartesian of cylindrical polar co-ordinate system impose a geometrical limitation on the solution. In particular, the application of the solid wall boundary conditions must involve interpolation between grid points not coincident with the boundaries. These limitations may adversely affect the accuracy of the solution, particularly in 'sensitive' areas of the flow, such as the leading edge regions. Consequently, it is anticipated that an improvement in accuracy may be achieved by the use of a boundary-fitted (curvilinear) co-ordinate system in which the geometrical limitations of the Cartesian or cylindrical systems may be removed and the wall boundary conditions can be applied more accurately. Such a co-ordinate system is adopted in the present study.

In the formulation of the SIMPLE algorithm, a staggered grid is generally implemented to eliminate the propagation of unphysical pressure oscillations. However, in the present study it was found that the staggered grid arrangement allowed localized pressure oscillations to persist adjacent to the periodic boundaries. These oscillations were found to be a consequence of the extended v-momentum control volumes which are required in this region as a result of the staggered storage locations. The need to use extended momentum control volumes may be removed by using non-staggered velocity locations. However, such storage allows pressure oscillations to develop in the whole of the flow domain, which outweighs the elimination of the localized oscillations. Nevertheless, there is a potentially more serious problem resulting from the use of staggered velocity locations in a boundary-fitted co-ordinate system. This is a consequence of the fact that the Cartesian velocity components (which remain the subject of the Navier–Stokes equation) are not related to the grid line orientations of the boundary-fitted system. In particular, the pressure gradients along the Cartesian axes are related to the pressure gradients along the boundary-fitted axes via the chain rule; the form of this relationship involving the grid line orientations. However, the staggering of the storage locations is directionally preferential, in that the staggered location for the u-velocity is designed to counter pressure oscillations in the x-direction of a Cartesian co-ordinate system, and similarly for the v-storage locations. Consequently, if the axes of the boundary-fitted system become highly skewed with the corresponding axes of the Cartesian system, the staggering of the storage locations has the incorrect directional preference and is no longer able to completely eliminate the pressure oscillations. This does not present a serious problem in the present boundary-fitted system; but, in the anticipated three-dimensional development of the code, such directional preference would pose serious difficulties in a centrifugal impeller, where there is a 90° curvature of the boundary-fitted axes.

Two schemes have formerly been proposed[7,8] for eliminating the pressure oscillations which arise with such non-staggered velocity locations. As a preliminary to three-dimensional impeller flows, these two schemes are applied to the incompressible flow through the two-dimensional NGTE 10C4/30C50 blade cascade, for which low-speed experimental results are available.[9] The aim of the present paper is, firstly, to compare the effectiveness of each scheme in eliminating the propagation of the pressure oscillations; and, secondly, to compare the flow computations of the most effective scheme with the experimental results for this cascade.

BOUNDARY-FITTED CO-ORDINATES

Transformation of the flow equations

The motion of a fluid is governed by a number of conservation equations (mass, momentum, etc.). In a (two-dimensional) Cartesian co-ordinate system these may be written in the form of a general transport equation for a dependent variable ϕ:

$$\frac{\partial(\rho u_j \phi)}{\partial x_j} = \frac{\partial}{\partial x_j}\left(\Gamma \frac{\partial \phi}{\partial x_j}\right) + S(x, y), \tag{1}$$

where Γ is the effective diffusion coefficient, $S(x, y)$ is the source term and there is a summation over the repeated index.

If a co-ordinate transformation $\xi = \xi(x, y), \eta = \eta(x, y)$ is introduced, equation (1) may be rewritten in the (ξ, η) co-ordinates as

$$\frac{\partial(\rho U_j \phi)}{\partial \xi_j} = \frac{\partial}{\partial \xi_j}\left(J\Gamma g^{jk} \frac{\partial \phi}{\partial \xi_k}\right) + S(\xi, \eta), \tag{2a}$$

where

$$U_j = (U, V),$$

$$U = J(\xi_x u + \xi_y v), \tag{2b}$$

$$V = J(\eta_x u + \eta_y v), \tag{2c}$$

$$g^{11} = \xi_x^2 + \xi_y^2, \tag{2d}$$

$$g^{12} = g^{21} = \xi_x \eta_x + \xi_y \eta_y, \tag{2e}$$

$$g^{22} = \eta_x^2 + \eta_y^2, \tag{2f}$$

$$J = x_\xi y_\eta - x_\eta y_\xi \tag{2g}$$

and $S(\xi, \eta)$ is the source term in the (ξ, η) co-ordinates.

The metrics ξ_x, etc. may be obtained from the derivatives x_ξ, etc. using the relationships

$$\xi_x = y_\eta / J, \quad \xi_y = -x_\eta / J, \tag{3a}$$

$$\eta_x = -y_\xi / J, \quad \eta_y = x_\xi / J. \tag{3b}$$

There are two similarities between equations (1) and (2a) that are worth noting:

(i) Both equations are written in the strong conservation law form. This means that a solution algorithm formulated in a Cartesian co-ordinate system may be directly transferred to the curvilinear system.

(ii) The dependent variable ϕ is the same in both equations. In particular, the transformed Navier–Stokes equations retain the Cartesian velocity components as the dependent variables. This is the semi-Cartesian form of the equations and is the most convenient form for the numerical computation.

The relationship between the physical (x, y) domain and the transformed (ξ, η) domain is illustrated in Figure 1.

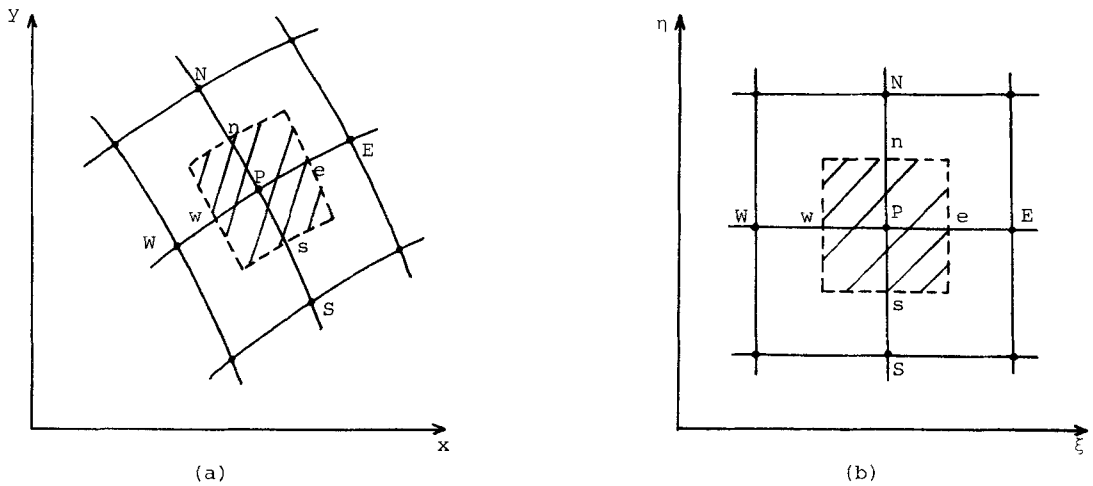

Figure 1. Finite difference grid: (a) physical plane; (b) transformed plane

Generation of the co-ordinate system

The boundary-fitted grid is generated using the Laplace formulation of Thompson and Mastin.[10] In this method the curvilinear co-ordinates (ξ,η) are generated as the solution of the elliptic equations

$$\alpha x_{\xi\xi} - 2\beta x_{\xi\eta} + \gamma x_{\eta\eta} = -J^2(Px_\xi + Qx_\eta), \tag{4a}$$

$$\alpha y_{\xi\xi} - 2\beta y_{\xi\eta} + \gamma y_{\eta\eta} = -J^2(Py_\xi + Qy_\eta). \tag{4b}$$

The solutions $x(\xi,\eta)$ and $y(\xi,\eta)$ of equation (4) give the Cartesian co-ordinates for each grid point. The coefficients α,β,γ are functions which depend on the grid line orientations, and the functions P and Q are exponential weighting functions which allow some input control of the grid point distribution. The resulting grid system for the NGTE 10C4/30C50 cascade is illustrated in Figure 2.

METHOD OF SOLUTION

General transport equation

To obtain a discretization of the flow field, the governing conservation equations are integrated around small control volumes surrounding each grid point. The resulting finite difference approximation for the general transport equation (2a) may be written as

$$(\rho U\phi\,\Delta\eta)_w^e + (\rho V\phi\,\Delta\xi)_s^n = (J\Gamma g^{11}\phi_\xi\,\Delta\eta)_w^e + (J\Gamma g^{22}\phi_\eta\,\Delta\xi)_s^n + S\,\Delta\xi\,\Delta\eta \tag{5}$$

where the 'cross-diffusion' terms involving g^{12} and g^{21} are taken into the discretized source term S. The grid point notation and a typical control volume are shown in Figure 1.

Equation (5) may be further manipulated in order to obtain a relation between ϕ_P and the values of ϕ at the surrounding grid points. This may be written as[6]

$$A_P\phi_P = A_N\phi_N + A_S\phi_S + A_E\phi_E + A_W\phi_W + S^\phi, \tag{6}$$

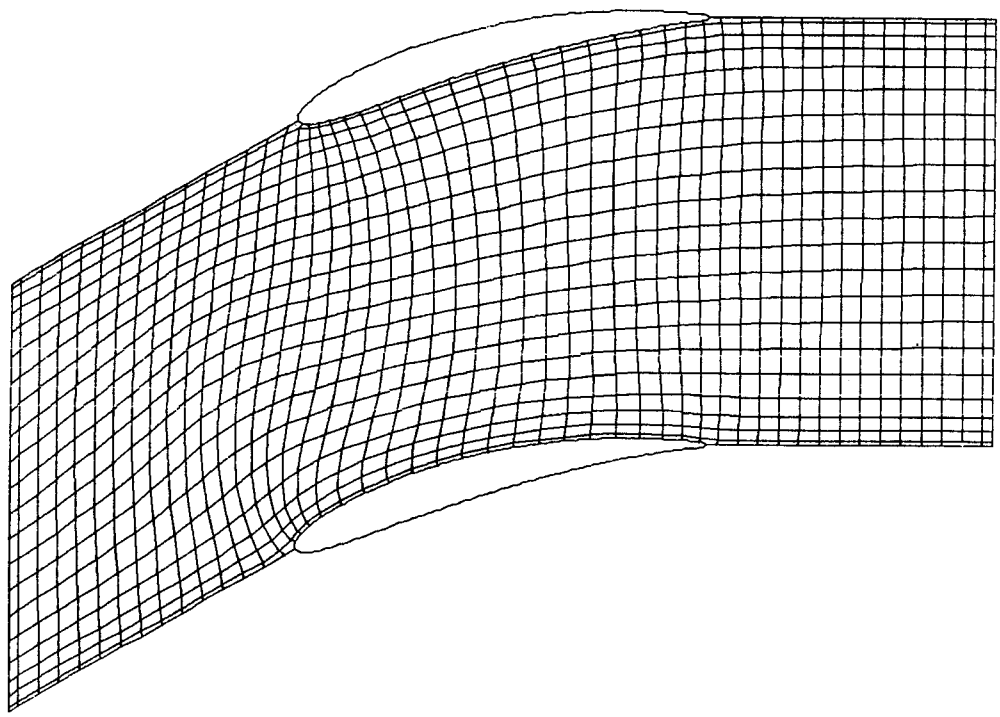

Figure 2. Boundary-fitted co-ordinate system for the NGTE 10C4/30C50 cascade

where the coefficients A involve the flow properties of diffusion and convection and the geometrical properties of the control cell. In the present elliptic scheme the diffusion terms are evaluated using a central difference and the convection terms using a first-order upwind difference.

For two-dimensional incompressible flow, the flow field is completely determined by the values of u, v, p (and μ). The values of u and v are determined as the solution of the momentum equations, which may be written as

$$u_{\mathrm{P}} = \sum_{\alpha} A_{\alpha} u_{\alpha} + S^{u} + (B^{u} p_{\xi} + C^{u} p_{\eta}), \tag{7a}$$

$$v_{\mathrm{P}} = \sum_{\alpha} A_{\alpha} v_{\alpha} + S^{v} + (B^{v} p_{\xi} + C^{v} p_{\eta}), \tag{7b}$$

where the α summation is over the grid points E, W, N, S;

$$B^{u} = -y_{\eta} \frac{\Delta\xi\,\Delta\eta}{A_{\mathrm{P}}}, \quad C^{u} = y_{\xi} \frac{\Delta\xi\,\Delta\eta}{A_{\mathrm{P}}}, \tag{7c}$$

$$B^{v} = x_{\eta} \frac{\Delta\xi\,\Delta\eta}{A_{\mathrm{P}}}, \quad C^{v} = -x_{\xi} \frac{\Delta\xi\,\Delta\eta}{A_{\mathrm{P}}}; \tag{7d}$$

and S^{u}, S^{v} are the appropriate source terms with the pressure gradient terms subtracted. (The coefficients A_{P} arising on the LHS of equations (7a) and (7b) have been incorporated into the terms on the RHS of each of these equations.)

If the correct pressure field were known in advance, then the simultaneous solution of equations (7a) and (7b) would deliver the correct values of u and v. However, the pressure values are not known and must be generated as part of the solution procedure.

Pressure correction equation

The solution of the pressure field is obtained using the SIMPLE procedure,[6] in which a guessed pressure field is iteratively updated using a series of pressure corrections. To illustrate this procedure, suppose that with a pressure field p^* the solution of the momentum equations yields u^* and v^*. Except in the converged solution u^* and v^* do not satisfy the continuity equation. To obtain satisfaction of both the momentum and continuity equations, suppose that the correct flow field (u, v, p) is obtained from the starred field by the addition of corrections (u', v', p'). Thus

$$u = u^* + u', \tag{8a}$$

$$v = v^* + v', \tag{8b}$$

$$p = p^* + p'. \tag{8c}$$

Since both u and u^* satisfy the momentum equation (7a) with pressure fields p and p^* respectively, the two forms of equation (7a) may be subtracted to give an equation relating u' to p';

$$u'_p = \sum_\alpha A_\alpha u'_\alpha + (B^u p'_\xi + C^u p'_\eta). \tag{9}$$

The first term on the RHS of this equation may be set to zero in the iterative part of the procedure, without influencing the converged solution.[6] Thus the corrected u-velocity is given by

$$u = u^* + (B^u p'_\xi + C^u p'_\eta). \tag{10a}$$

Similarly, the corrected v-velocity is

$$v = v^* + (B^v p'_\xi + C^v p'_\eta). \tag{10b}$$

Hence the corrections to the curvilinear velocity components may be obtained from equations (2b) and (2c):

$$U = U^* + (B^u y_\eta - B^v x_\eta) p'_\xi + (C^u y_\eta - C^v x_\eta) p'_\eta, \tag{11a}$$

$$V = V^* + (C^v x_\xi - C^u y_\xi) p'_\eta + (B^v x_\xi - B^u y_\xi) p'_\xi, \tag{11b}$$

where U^* and V^* are based on u^* and v^*.

The last two terms of equations (11a) and (11b) represent 'cross' pressure derivatives, which do not arise in a Cartesian co-ordinate system. However, since the pressure correction equation is to be solved using a successive line procedure, these terms may be set to zero. This does not influence the converged solution, in which $p' = 0$. Hence the corrections to the transformed velocity components are

$$U = U^* + Bp'_\xi, \tag{12a}$$

$$V = V^* + Cp'_\eta, \tag{12b}$$

where

$$B = B^u y_\eta - B^v x_\eta, \quad C = C^v x_\xi - C^u y_\xi. \tag{12c}$$

Finally, substituting equations (12a) and (12b) into the continuity equation yields an equation for the pressure correction:

$$(\rho B p'_\xi \Delta\eta)^{\mathrm{e}}_{\mathrm{w}} + (\rho C p'_\eta \Delta\xi)^{\mathrm{n}}_{\mathrm{s}} + m_{\mathrm{p}} = 0, \tag{13}$$

where m_{p} is the integrated mass source

$$m_{\mathrm{p}} = \int_{\Delta\xi}\int_{\Delta\eta}\left(\frac{\partial(\rho U^*)}{\partial\xi} + \frac{\partial(\rho V^*)}{\partial\eta}\right)\mathrm{d}\xi\,\mathrm{d}\eta. \tag{14}$$

Using central differencing to obtain the pressure derivatives across the cell boundaries,[6] equation (13) becomes

$$A^{\mathrm{P}}_{\mathrm{P}} p'_{\mathrm{P}} = A^{\mathrm{P}}_{\mathrm{N}} p'_{\mathrm{N}} + A^{\mathrm{P}}_{\mathrm{S}} p'_{\mathrm{S}} + A^{\mathrm{P}}_{\mathrm{E}} p'_{\mathrm{E}} + A^{\mathrm{P}}_{\mathrm{W}} p'_{\mathrm{W}} - m_{\mathrm{p}}, \tag{15}$$

where the coefficients A involve B, C, ρ, etc.

Equation (15) may be solved to obtain values for p', and hence the corresponding velocity corrections may be evaluated.

Solution procedure

The system of governing finite difference equations was solved using a successive line underrelaxation (SLUR) method, in which the Tridiagonal Matrix Algorithm (TDMA)[5] was applied to each equation in turn. The flow equations were solved on successive cross-stream lines which marched from the inlet to the outlet of the cascade. The elliptic nature of the flow was accounted for by repeating complete sweeps of the flow field until a converged solution was obtained.

The numerical solutions on each cross-stream line were obtained using the SIMPLE algorithm[6] adapted to the boundary-fitted co-ordinate system. In this procedure an estimated pressure field p^* yields an intermediate solution (u^*, v^*) to the momentum equations. From these values the curvilinear velocity components are updated. If these velocities do not satisfy the mass conservation law, the required adjustments to the pressure and velocity fields are calculated from the pressure correction equation. This completes one cross-stream cycle of computation which is then repeated on the next cross-stream station. Finally, the viscosity values were updated, at the end of each complete sweep of the flow field, using the algebraic procedure of Baldwin and Lomax.[11] This form of turbulence model was chosen in preference to the k–ε model, since the algebraic equations are much quicker to evaluate than the two transport equations required in the k–ε procedure. (This consideration is expected to be particularly important in the three-dimensional development of the present code.)

VELOCITY STORAGE LOCATIONS

In the formulation of the SIMPLE algorithm consideration must be given to the propagation of unphysical oscillations in the pressure field. In general, these may be eliminated with the use of a staggered grid. However, in the present study it was found that this formulation failed to deliver a pressure field which satisfied the periodicity condition on the open boundaries of the flow domain. In particular, it was found that on lines of ξ = constant the converged pressure values on either side

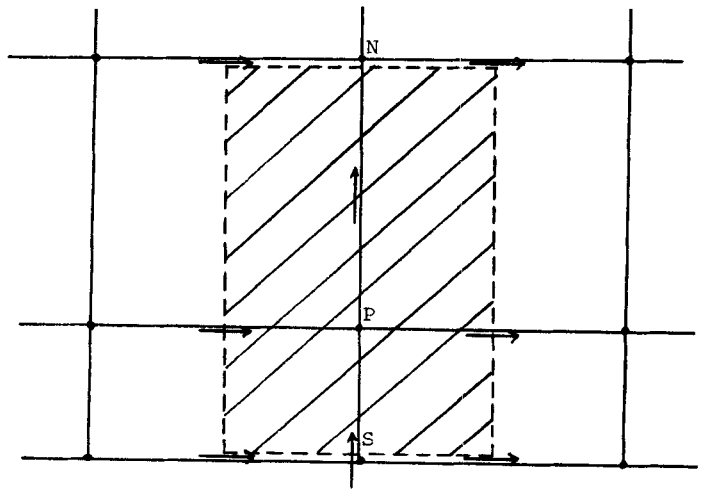

Figure 3. Lower boundary v-momentum control volume in a staggered grid formulation: →, u, U storage location; ↑, v, V storage locations; ●, pressure storage locations

of the periodic boundary became highly skewed with each other and with the interior pressure values. However, the average of the two skewed values gave a value on the periodic boundary which was consistent (in terms of a smoothly varying field) with the interior pressure values. Further, on each ξ = constant line the two skewed pressure values were consistent with the corresponding skewed values on the adjacent ξ = constant lines. (Adjacent to the blade surfaces, this skewing of the pressure values did not occur.)

This localized oscillation was found to be a consequence of the extended v-momentum control volumes that are required at the north and south boundaries of the solution domain. A typical control volume of this type is illustrated in Figure 3. For this cell the pressure gradient in the η-direction may be calculated independently of the pressure value which is stored in the interior of the cell. Hence these pressure values are only constrained to give a smoothly varying pressure field in the ξ-direction. In the η-direction the pressure field is constrained only by the pressure boundary condition.

Where the flow is bounded by a solid wall, the pressure boundary condition is taken to be $\partial p/\partial \eta = 0$. Hence the pressure values on the solid boundary are a direct extrapolation of the values adjacent to the wall, which suppresses any localized oscillation in the η-direction. However, where the flow is bounded by the periodicity condition, the pressure on the boundary is obtained from the average of the values on either side of the boundary. Hence the two pressure values may become highly skewed but, provided they give the correct average and are consistent in the ξ-direction, the velocity field will not be able to sense the oscillation. Since the solution of the pressure field is generated by a series of corrections, the pressure correction equation is also unable to sense the oscillation.

It would, perhaps, be anticipated that the consistency requirement in the ξ-direction would limit the extent of any skewness of the pressure values. However, in the interior of the blade passage there is a pressure difference (loading) across the blade. Consequently, at the change in the boundary conditions (from periodic to solid wall) the consistency in the ξ-direction is not sufficient to suppress the localized oscillation. This is particularly so at the leading edge, where the flow accelerates rapidly to give a large loading; whereas, at the trailing edge there is an unloading of the blade (Kutta condition). Thus, as was experienced in the present solution, the localized oscillation is more severe on

the periodic boundary upstream of the leading edge than it is on the boundary downstream of the trailing edge.

This inadequacy of the staggered grid arrangement to deliver a periodicity-satisfying pressure field has previously been experienced in the two-dimensional cascade analysis of Mirzabozorg.[12] In this case a Cartesian co-ordinate system was used, and to achieve the required pressure periodicity, Mirzabozorg proposed a joint SIMPLE/SIMPLER scheme in which the SIMPLER procedure[13] was implemented outside the blade passage (to 'force' the periodicity) and the SIMPLE procedure was retained inside the blade passage.

In the boundary-fitted co-ordinate system the staggering of the velocity locations is further made undesirable (as discussed in the Introduction to this study) because the Cartesian velocity components are no longer related to the grid line orientations of the co-ordinate system. Consequently, to resolve this problem in the boundary-fitted co-ordinates, a scheme is sought in which the velocity components may be stored on a set of non-staggered locations. In this case careful consideration must be given to the pressure correction scheme, since the non-staggered velocity locations no longer suppress the propagation of global pressure oscillations. Two schemes are considered for the elimination of these oscillations.[7,8] The first continues to store the pressure on a set of staggered locations, whereas the second uses a completely non-staggered set of storage locations.

STAGGERED PRESSURE LOCATIONS

Two positions were considered for the pressure storage locations:

(*a*) *The velocity components are stored at the cell centres with the pressure stored at the cell corners*

The structure of this grid (illustrated in Figure 4(i)), by its nature, is not sufficient to eliminate the propagation of pressure oscillations. Such oscillations arise in the diagonal directions, since the pressure values are not known at the central points on the cell boundaries and must be obtained by interpolation between the values at the corner storage locations.

In an attempt to eliminate these oscillations, the method proposed by Vanka *et al.*[7] was implemented. In this method an amended procedure for generating the p' values is used. Rather than solving equation (15) for p', which would not eliminate the diagonal pressure oscillations, a cell-by-cell procedure is used in which it is supposed that at each pressure location all the surrounding values of p' are zero (which is valid in the converged solution). Thus equation (15) reduces to

$$p'_{\mathrm{P}} = -m_{\mathrm{P}}/A_{\mathrm{P}}. \tag{16}$$

Equation (16) generates a pressure correction for each cell independently of the surrounding p' values. The size of the p' correction depends on the size of the continuity error m_{P}. Thus to generate a converged solution with this procedure, the values of p' are used to update the velocity values, which allow a new continuity error to be generated. With the new mass sources the values of p' may be recalculated. The velocities are again corrected and the sequence is repeated (up to a maximum of 10 times, as suggested by Vanka *et al.*[7]) until the continuity errors are acceptably small.

The rationale of this procedure relies on the fact that the velocities are corrected using a 1-δ gradient of p' (whereas the p-gradients in the momentum equations are based on 2-δ differences). Thus by repeatedly calculating the mass sources the flow field is forced to 'feel' the 1-δ gradients. The only shortcoming in this procedure is that the velocity field can only sense the 1-δ variations in

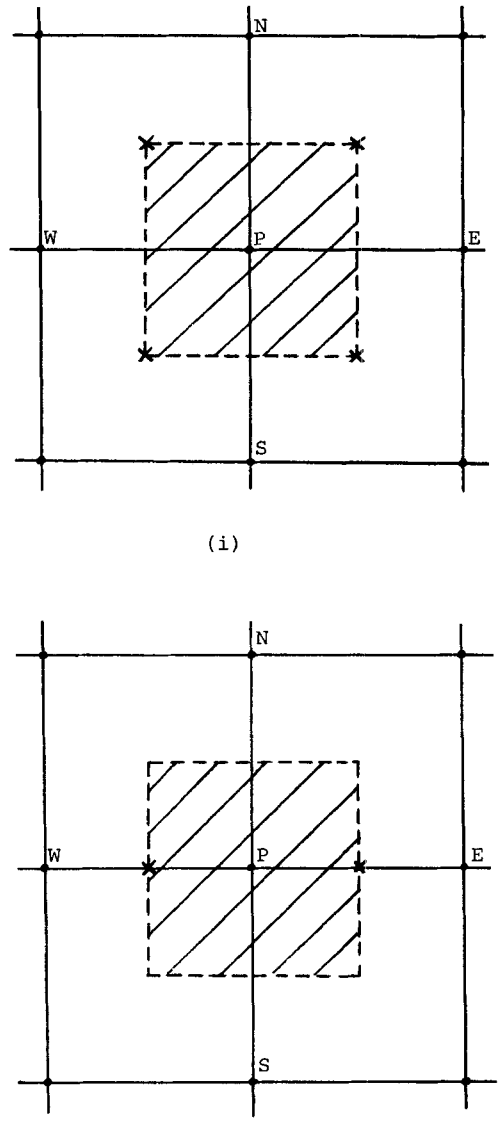

Figure 4. Staggered pressure storage locations: (i) scheme (a); (ii) scheme (b); ●, velocity storage locations; ×, pressure storage locations

p' and not in p. Thus if an oscillatory pressure field arose during the course of the solution, this procedure would not be able to respond to it. The success of the method relies in restricting the development of an oscillatory pressure field from the outset of the iterative procedure.

With this method implemented, it was found that the diagonal pressure oscillations persisted within the open channel, but within the interior of the blade passage the oscillations were successfully suppressed. (Some oscillations did occur inside the blade passage, but these decayed

rapidly and were restricted to the leading and trailing edge regions, where there was a border with the open passage. These were considered to be oscillations from the open boundary which were able to penetrate a small distance into the blade passage.) This dual nature of the pressure field appears to be a consequence of the dual boundary conditions within the cascade. It is anticipated that the pressure oscillations may be especially persistent in the leading and trailing edge regions, where the satisfaction of the continuity equation is most difficult to achieve. Further, it may be argued that the solid wall condition at the blade surfaces does not allow the pressure oscillations to 'cross' the boundary, and so any oscillations are suppressed; whereas the periodicity condition at the open boundaries allows the pressure oscillations the freedom to persist across the boundary, and consequently the oscillations are not suppressed in this region of the flow.

Attempts to remove the pressure oscillations centred on smoothing the values of p' in the open regions of the cascade. This operation is justified by the fact that in the converged solution the p' values all approach zero; thus a small manipulation of the p' values during the iterative procedure ought not to influence the final solution. The values of p' were smoothed according to the linear relationship

$$(p'_{\mathrm{P}})_{\mathrm{smoothed}} = p'_{\mathrm{P}} - \alpha[p'_{\mathrm{P}} - \tfrac{1}{2}(p'_{\mathrm{N}} + p'_{\mathrm{S}})], \tag{17}$$

where α represents the degree of smoothing ($0 \leqslant \alpha \leqslant 1$).

Since the governing equations were solved using a line-by-line procedure, the p' values were only smoothed in the cross-stream (η) direction. However, due to the diagonal nature of the pressure oscillations, this smoothing was not able to completely remove the oscillations. But, rather than attempting a more complicated procedure, involving some form of smoothing in the ξ-direction, an alternative method of staggering is implemented. The structure of this grid is designed to eliminate the oscillations in the ξ-direction, while the above scheme is used to counter the oscillations in the η-direction.

(*b*) *In the second grid the pressure storage locations are only staggered in the ξ-direction*

Using this grid (illustrated in Figure 4(ii)) the pressure gradients in the ξ-direction are evaluated by a 1-δ difference, but in the η-direction a 2-δ difference is still used. Thus this grid allows the possibility of pressure oscillations in the η-direction, but in the ξ-direction the 1-δ difference suppresses any pressure oscillations, as in the original staggered grid. Hence smoothing in the η-direction ought to be more successful with this type of grid. This was indeed found to be the case. However, the optimum smoothing factor ($\alpha = 0{\cdot}5$) was required in the open passage in order to achieve a non-oscillatory pressure field. Within the blade passage, where the oscillations are restricted to the border regions with the open boundaries, a much smaller smoothing factor was required ($\alpha = 0{\cdot}1$).

To obtain an indication of the validity of the results obtained using this procedure, the pressure coefficient along the blade surfaces was computed and compared with the available experimental values.[9] These results are presented in Figure 5 and show an acceptable correspondence between the predicted and experimental values.

The applicability of this method is felt to be limited for two reasons: firstly, because the method cannot respond to and correct any pressure oscillations that do persist in the solution; secondly, because the only way to eliminate the oscillations completely is to use a large amount of smoothing in the open channel. For this reason an alternative procedure was implemented, in which a completely non-staggered grid was used.

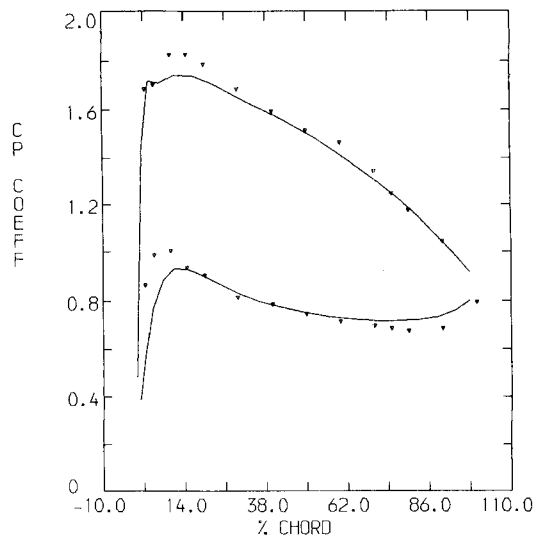

Figure 5. Comparison of the experimental pressure coefficient with the computed coefficient, using pressure correction equation (16): V, experimental,[9] solid curve, calculated

NON-STAGGERED PRESSURE LOCATIONS

Rhie and Chow pressure correction scheme

In order to eliminate the global pressure oscillations that arise from the use of a non-staggered grid, the method of Rhie and Chow[8] was considered. The rationale of this procedure is based on the observation that when the mass fluxes are evaluated for the pressure correction equation, the values of u and v(or U and V) used in the evaluation are the values on the cell boundaries rather than the values at the grid points. The usual procedure would be to obtain the boundary values by a simple averaging of the grid point values. Such an averaging would be partly responsible for the development of an oscillatory pressure field. Rhie and Chow's modification is based on the supposition that if the velocity values at the cell boundaries were obtained by solving the momentum equations applied at the boundary points, then these momentum equations would contain pressure gradients which could be evaluated as the difference between neighbouring pressure locations.

To illustrate this procedure, suppose the momentum equations (7a) and (7b) are substituted directly into equation (2b). This produces an equation for the U-velocity:

$$U^* = \tilde{U} + B\frac{\partial p^*}{\partial \xi}, \tag{18}$$

where $\tilde{U}$ contains all the terms arising from the above substitution except for the pressure gradient in the ξ-direction.

Consider the eastern boundary of a typical control volume (point e in Figure 1). In the application of the mass continuity law, the value of U at point e is required. If this value were obtained directly from the solution of equation (18) at point e, then the pressure gradient in this equation could be evaluated using a 1-δ difference between the pressure values at the grid points P and E. However, equation (18) can only be applied at points P and E, at which the pressure

gradients are evaluated using a 2-δ difference. The value of U_e^* is then obtained from the average of U_P^* and U_E^*. Using equation (18) in the evaluation of this average gives

$$U_e^* = \frac{1}{2}\left[(\tilde{U}_P + \tilde{U}_E) + B_P\left(\frac{\partial p^*}{\partial \xi}\right)_P + B_E\left(\frac{\partial p^*}{\partial \xi}\right)_E \right]. \tag{19a}$$

This equation may be re-expressed as

$$\bar{U}_e^* = \tfrac{1}{2}(\tilde{U}_P + \tilde{U}_E) + \bar{B}_e \bar{p}_\xi^*, \tag{19b}$$

where the over-bar denotes results obtained using central differencing between the grid points.

Approximating $\tilde{U}_e$ by the average of the values at P and E and rearranging equation (19b) gives

$$\tilde{U}_e = \bar{U}_e^* - \bar{B}_e \bar{p}_\xi^*. \tag{19c}$$

Finally, substituting this equation into equation (18) applied at the eastern boundary gives

$$U_e^* = \bar{U}_e^* + \bar{B}_e\left[\left(\frac{\partial p^*}{\partial \xi}\right)_e - \bar{p}_\xi^* \right]. \tag{19d}$$

Similar formulations are used for U_w^*, V_n^*, V_s^*.

As can be seen, the usual averaging to obtain the velocity values on the cell boundaries contains an additional term which represents the difference between the 1-δ and 2-δ difference schemes for the pressure gradient. Thus if an oscillatory pressure field were to arise, the magnitude of this term would be large and would act to remove the oscillation; whereas for the required non-oscillatory field the magnitude of this term remains small.

In the current scheme the pressure correction equation was used in a slightly amended form of that proposed by Rhie and Chow.

Current pressure correction scheme

In the formulation of the pressure correction equation using equation (19d), it is observed that some of the additional terms that arise are in a form which allows the equation to be written in terms of p rather than p'. This does not alter the pressure correction equation, but merely re-expresses it.

On substituting equation (19d) into equation (12a), the resulting correction to the U-velocity is

$$U_e = \bar{U}_e^* + \bar{B}_e\left[\left(\frac{\partial p^*}{\partial \xi}\right)_e - \bar{p}_\xi^* \right] + \bar{B}_e\left(\frac{\partial p'}{\partial \xi}\right)_e. \tag{20a}$$

The 1-δ gradients of p^* and p' in this equation may be added to give a 1-δ gradient in p:

$$U_e = \hat{U}_e + \bar{B}_e\left(\frac{\partial p}{\partial \xi}\right)_e, \tag{20b}$$

where

$$\hat{U}_e = \bar{U}_e^* - \bar{B}_e \bar{p}_\xi^*, \tag{20c}$$

with similar expressions for U_w, V_n, V_s.

Substituting these expressions into the continuity equation in the usual way gives

$$A_P^p p_P = \sum_\alpha A_\alpha^p p_\alpha - m_P, \tag{21}$$

where m_p is the integrated mass source based on the 'pseudo' velocities $\hat{U}$ and $\hat{V}$. This equation may

be solved to give both the updated pressure values and, consequently, the p' values required to update the velocity values.

It is important to remember that although equation (21) solves directly for p, the method is still SIMPLE-based rather than SIMPLER-based. This can be illustrated by considering an initial guess in which the velocities exactly satisfy continuity but the pressure field (incorrectly) has a constant value everywhere in the flow domain. In this case equation (21) would not adjust the pressure field until the solution of the momentum equations had delivered a flow field which did not satisfy continuity. Thus, in common with the SIMPLE procedure, the pressure correction in this scheme is 'driven' by errors in the mass conservation law.

For the present cascade studies the pressure correction equation in terms of p is felt to have advantages over the corresponding equation in terms of p'. (The two equations are exactly the same except that one is a rearrangement of the other.) This formulation allows the periodicity condition to be implemented directly as a boundary condition for the pressure correction equation. With this formulation it was found that the pressure oscillations were eliminated in all regions of the cascade.

RESULTS AND DISCUSSION OF FLOW COMPUTATIONS

The flow equations were discretized on a 50×20 grid, with 20 grid points placed in the spanwise direction and 20 points spaced along each blade surface. In each case considered approximately 300 iterations were required in order to achieve a converged solution, taking about 1 h 30 min of CPU time on a Perkin Elmer 3210 computer.

The solution procedure was used to evaluate four sets of salient flow data for the cascade. These were: the pressure coefficient along the blade surfaces; the variation of the deviation and deflection angles with incidence; and the variation of the deviation angle with the cascade solidity.

Pressure coefficient

The blade pressure coefficient was computed for an inlet flow angle of 30°, with zero incidence and a cascade solidity of one. The comparison between the computed and experimental coefficients is shown in Figure 6.

The calculated values do not quite achieve the same peak values near the leading edge as the experimental values. This is due to the 'bluntness' of the leading edge and the large flow gradients associated with this region. However, the calculated values do show the same qualitative shape as the experimental results, especially on the suction surface. The rapid fall in the calculated values of C_P as the first (leading edge) grid point on each blade surface is approached is also felt to be due to the large flow gradients in the leading edge region, but also the computational grid was constructed with two grid points on each surface closer to the leading edge than the first experimental point. Disregarding these points (which is arguably valid since there are no experimental values in this region) would remove the rapid fall in the C_P values and give a much better qualitative agreement with the experimental results.

Along the remainder of the blade surface the calculated and experimental values are in good agreement. The calculated values approach the Kutta condition at the trailing edge, but do not achieve it exactly since the grid points are displaced from the trailing edge point on the blade.

Variation of deviation and deflection with incidence

The deviation angle is the difference between the outlet flow angle and the blade mean line angle

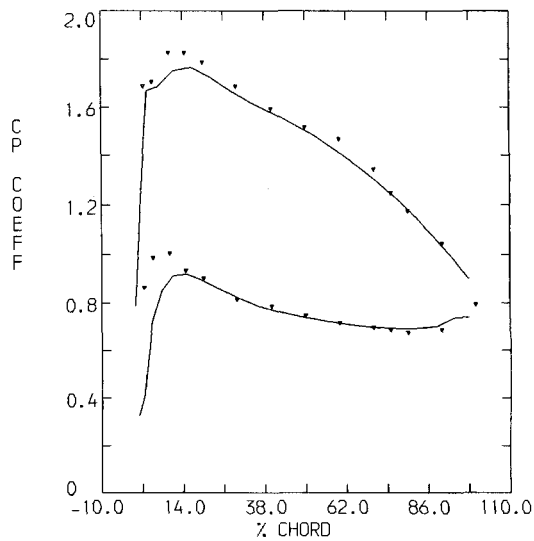

Figure 6. Comparison of the experimental pressure coefficient with the computed coefficient, using pressure correction equation (21): ∇, experimental,[9] solid curve, calculated

at the trailing edge. This angle is a measure of how well the cascade 'guides' the flow and is dependent on such factors as the cascade geometry and the incidence angle of the flow. The existence of the deviation angle arises largely as a result of the boundary layer growth along the blade surfaces. (The deflection angle is the difference between the inlet and outlet flow angles.)

Felix and Emery[9] reported experimental values for the variation of deflection and deviation with incidence angle. Numerical solutions were obtained with the proposed code for a range of incidence angles, and the computed deflection and deviation angles were evaluated. The comparisons of these results with the experimental results are shown in Figures 7 and 8 respectively.

These results again show a good qualitative agreement with the experimental values, although the computed results are slightly displaced from the experimental results. In the case of the deflection angle, the calculated results show the same linear profile as the experimental results in the range $-8{\cdot}0° <$ incidence $< 4{\cdot}0°$. The calculated values also show the same move away from the linear profile for the larger positive values of incidence angle, although the magnitude of the move is underachieved in the numerical results. A similar qualitative agreement is obtained when the deflection angle values are used to give the variation of deviation angle with incidence.

Variation of deviation with solidity

Following Wang *et al.*,[14] the computed variation of deviation angle with solidity, obtained using the proposed code, is compared with data from empirical correlations (which are derived from a number of experimental results) rather than with the results from an individual experimental study. There are two such correlations in common use; the first is Carter's rule and the second is the NASA correlation.[15]

For Carter's rule the deviation angle δ is given by[15]

$$\delta = m\phi/\sqrt{\sigma}, \tag{22a}$$

where σ is the cascade solidity, ϕ is the camber angle and m is a factor of proportionality which varies with the blade setting angle.

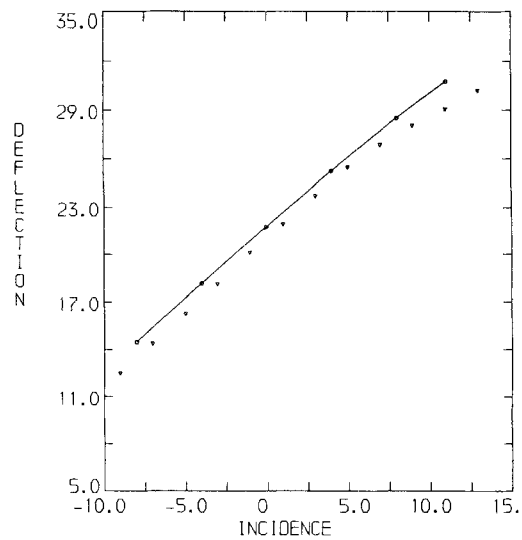

Figure 7. Comparitive variation of deflection angle with incidence angle for cascade solidity = 1:∇, experimental;[9] solid curve, calculated

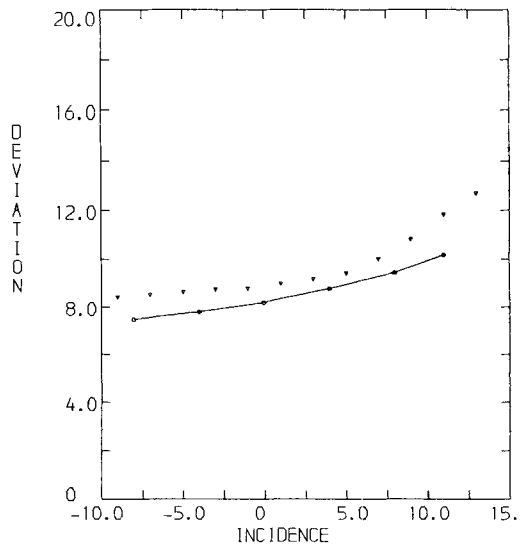

Figure 8. Comparitive variation of deviation angle with incidence angle for cascade solidity = 1: ∇, experimental;[9] solid curve, calculated

For NASA's rule the deviation angle is given by[15]

$$\delta = \delta_0 + m\phi/\phi^b, \tag{22b}$$

where δ_0, m and b vary with the inlet flow angle.

Numerical results were obtained for a range of values of solidity (all with an inlet flow angle of 30° and zero incidence), and the comparison with the above correlations is shown in Figure 9.

The computed results show a much better agreement with the NASA correlation than with Carter's correlation. However, since the two correlations do not give exactly similar values for the

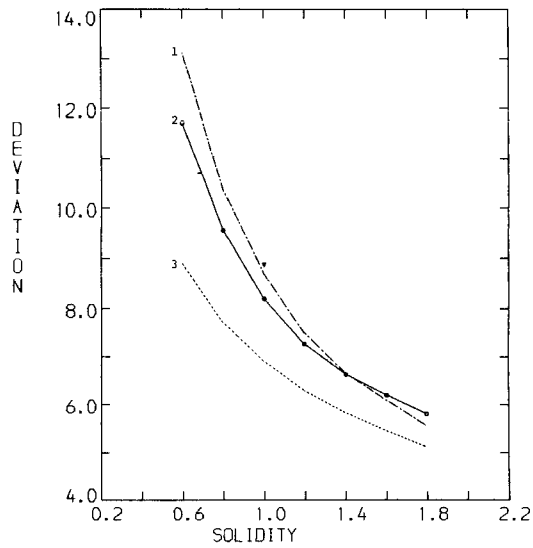

Figure 9. Comparitive variation of deviation angle with cascade solidity for blade setting angle = 15° and zero incidence angle: 1, NASA correlation;[15] 2, calculated; 3, Carter's rule;[15] ∇, zero-incidence experimental deviation from Figure 8.

variation of deviation with solidity, the approximate agreement of the computed variation with the NASA correlation is felt to be acceptable.

It is interesting to note that in Figures 7 and 8 the zero-incidence conditions correspond to the unity-solidity condition in Figure 9. To illustrate this, the experimental value of deviation at zero incidence, from Felix and Emery,[9] is also plotted in Figure 9. This experimental point is in very close agreement with the corresponding point from the NASA correlation, but not in such good agreement with that from Carter's correlation. Thus at this isolated point the closer agreement of the computed deviation with the NASA correlation is favourable.

CONCLUSIONS

A boundary-fitted co-ordinate system is used in the development of a solution procedure, based on the SIMPLE algorithm,[6] in which the velocity locations are non-staggered. The consequent pressure oscillations are eliminated using a modified form of the scheme proposed by Rhie and Chow.[8]

The solution procedure is used to calculate the low-speed flow through a two-dimensional cascade, using an algebraic turbulence model.[11] Good overall agreement is obtained with the available experimental results[9] and correlations.[15]

ACKNOWLEDGEMENTS

The author would like to express his thanks to Professor R. L. Elder and Dr. M. Lobo for many useful discussions and comments on the preparation of this paper; and to M. Mirzabozorg and Dr F. Alamdari for many useful discussions on the application of the SIMPLE algorithm.

REFERENCES

1. C. H. Wu, 'A general theory of three-dimensional flow in subsonic and supersonic turbomachines of axial, radial and mixed flow types', *NACA-TN-2604*, 1952.

2. C. Bosman, 'Analytical theory of three dimensional flow in centrifugal compressors', *J. Mech. Eng. Sci.*, **23** (4), 179–191 (1981).
3. J. D. Denton, 'A time marching method for two- and three-dimensional blade to blade flow', *ARC R&M 3775*, 1974.
4. J. Moore and J. G. Moore, 'Calculations of three-dimensional, viscous flow and wake development in a centrifugal impeller', '*Performance Prediction of Centrifugal Pumps and Compressors*', ASME, 1980.
5. W. M. Pun and D. B. Spalding, 'A general computer program for two-dimensional elliptic flows', *Report HTS/76/2*, Imperial College (London), Mechanical Engineering Department, Amended 1977.
6. S. V. Patankar and D. B. Spalding, 'A calculation procedure for heat, mass, momentum transfer in three-dimensional parabolic flows', *Int. J. Heat Mass Transfer*, **15**, 1787–1806 (1972).
7. S. P. Vanka, B. C.-J. Chen and W. T. Sha, 'A semi-implicit calculation procedure for flows described in boundary-fitted coordinate systems', *Numer. Heat Transfer*, **3**, 1–19 (1980).
8. C. M. Rhie and W. L. Chow, 'Numerical study of the turbulent flow past an aerofoil with trailing edge separation', *AIAA J.*, **21** (11), pp. 1525–1532 (1983).
9. A. R. Felix and J. C. Emery, 'A comparison of typical national gas turbine establishement and NACA axial-flow compressor blade sections', *NACA-TN-3937*, 1957.
10. J. F. Thompson and C. W. Mastin, 'Grid generation using differential systems', *NASA CP 2166 Numerical Grid Generation Techniques*, 1980.
11. B. S. Baldwin and H. Lomax, 'Thin layer approximation and algebraic model for separated turbulent flows', *AIAA Paper No. 78-257*, 1978.
12. M. A. S. Mirzabozorg, Private Communication, Cranfield Institute of Technology, 1985.
13. S. V. Patankar, *Numerical Heat Transfer and Fluid Flow*, Hemisphere Publications, New York, 1980.
14. L. C. Wang, R. Hetherington and A. Goulas, 'The calculation of deviation angle in axial-flow compressor cascades', *ASME Paper 82-GT-230*, 1982.
15. 'Aerodynamic design of axial-flow compressors', *NASA SP-36*, 1965.